Materials & Design 264 (2026) 115736

Contents lists available at ScienceDirect

Materials & Design

journal homepage: www.elsevier.com/locate/matdes

Smart multifunctional hydrogels with shape memory, conductivity, self-healing, and adhesive properties for biomedical applications

Ha Huong [a,b,1], Cuong Hung Luu [c,d,1], V.H. Giang Phan [a,1], Gopinathan Janarthanan [e], Ngoc-Thuy Huynh [a], Hieu Trung Nguyen [a], Nhu-Y Ngoc Ha [a], Hang Thu Ta [c,d], Qihui Zhou [f], Sanjairaj Vijayavenkataraman [e,g,*], João Conde [h,**], Thavasyappan Thambi [i,j,***]

[a] Biomaterials and Nanotechnology Research Group, Faculty of Applied Sciences, Ton Duc Thang University, Ho Chi Minh City, Vietnam
[b] Department of Advanced Materials Engineering, Kangwon National University, Samcheok 25931, the Republic of Korea
[c] School of Environment and Science, Griffith University, Nathan, QLD 4111, Australia
[d] Queensland Quantum and Advanced Technologies Research Institute, Griffith University, Nathan, QLD 4111, Australia
[e] The Vijay Lab, Division of Engineering, New York University Abu Dhabi, Abu Dhabi, United Arab Emirates
[f] Shandong Engineering Research Center for Tissue Rehabilitation Materials and Devices, School of Rehabilitation Sciences and Engineering, University of Health and Rehabilitation Sciences, Qingdao 266071, China
[g] Department of Mechanical and Aerospace Engineering, Tandon School of Engineering, New York University, Brooklyn, NY 11201, USA
[h] Comprehensive Health Research Centre (CHRC), NOVA Medical School|Faculdade de Ciências Médicas, NMS|FCM, Universidade Nova de Lisboa 1169-056 Lisboa, Portugal
[i] Graduate School of Biotechnology, College of Life Sciences, Kyung Hee University, Yongin si, Gyeonggi do 17104, the Republic of Korea
[j] Department of Marine Biotechnology, AMET University, Chennai 603112, Tami Nadu, India

ARTICLE INFO

Keywords:
Shape memory hydrogels
Stimuli-responsive materials
Self-healing
Controlled release

ABSTRACT

Shape memory hydrogels often suffer from slow recovery, mechanical weakness, and poor stability under physiological environments, limiting their biomedical applicability. Herein, we developed a multifunctional smart hydrogel composed of gelatin, chitosan, alginate, and montmorillonite clay (GCAM), engineered for advanced biomedical applications. The hydrogel exhibited ion-responsive shape memory behavior, through calcium-mediated "egg-box" fixation and bicarbonate-induced recovery, achieving robust recovery of complex geometries. GCAM hydrogels showed a high swelling ratio (324.1 ± 22.4%), an interconnected porous structure, excellent skin adhesiveness without leaving residue, and controlled degradation (14.1 ± 0.3% weight loss by day 20 and 85.4 ± 2.1% by day 60 in PBS). The material exhibited rapid self-healing (≤ 1 h), recovering ~90% tensile strength and maintaining electrical conductivity to enabling LED illumination in a closed circuit. Enoxaparin was successfully encapsulated and released in a sustained manner over 14 days, with cumulative release of 91.6 ± 5.4%. The hydrogel showed strong biocompatibility with viability exceeding 80% at 80 μg/mL in mouse vascular endothelial cells, alongside excellent hemocompatibility, and the promotion in vascularization in the CAM assay. Collectively, these findings highlight the multifunctional potential of the GCAM hydrogel for advanced biomedical and wearable applications.

1. Introduction

The development of shape memory materials has long focused on metals such as nickel-titanium (NiTi) and copper–aluminum-nickel (CuAlNi), which have been widely studied because of their unique ability to recover a predefined shape when subjected to specific stimuli

* Corresponding author at: The Vijay Lab, Division of Engineering, New York University Abu Dhabi, Abu Dhabi, United Arab Emirates.
** Corresponding author.
*** Corresponding author at: Graduate School of Biotechnology, College of Life Sciences, Kyung Hee University, Yongin si, Gyeonggi do 17104, the Republic of Korea.
E-mail addresses: phanvuhoanggiang@tdtu.edu.vn (V.H.G. Phan), vs89@nyu.edu (S. Vijayavenkataraman), joao.conde@nms.unl.pt (J. Conde), thambi@khu.ac.kr (T. Thambi).
[1] These authors contributed equally to this work.

https://doi.org/10.1016/j.matdes.2026.115736
Received 26 September 2025; Received in revised form 18 February 2026; Accepted 24 February 2026
Available online 25 February 2026

such as heat or pressure [1–3]. These metal-based shape memory alloys (SMAs) have been applied in diverse fields, including biomedical devices such as orthodontic wires, stents, bone fixation implants, and surgical instruments [4]. However, SMAs have limitations, especially in biomedical contexts, owing to potential biocompatibility issues, restrictions on stimuli activation within the human body, and the risk of toxic degradation products over time [4,5]. Additionally, their rigid structures can lead to issues such as inflammation, thrombosis, or unwanted immune responses when used for devices that contact the blood vessels [6,7]. These disadvantages have motivated the development of alternative materials that can provide similar functionality while overcoming the limitations of metals.

Shape memory hydrogels (SMHs) represent a promising alternative to metal-based SMAs, particularly in biomedical applications [8–10]. Hydrogels made from biocompatible polymers exhibit several outstanding properties. They are bio-friendly, easily modifiable, and capable of carrying therapeutic agents, thereby enhancing the effectiveness of treatments [11–14]. SMHs can respond to various stimuli, such as heat, light, magnetic fields, or electricity, making them ideal candidates for controlled drug release systems and other medical applications [15]. However, the practical applications of SMHs are often limited by the nature of their stimuli. Many of the stimuli required to trigger the shape memory effect are not easily applicable within the human body, or they require complex external systems to activate, which may limit their utility in minimally invasive medical treatments [15–17].

Synthetic polymers have been at the forefront of SMHs research, especially those that can respond to external stimuli such as temperature and pressure changes. Polymers such as poly(N-isopropylacrylamide) and poly(cyclooctene) have shown potential for shape memory applications [15]. However, despite their advantageous properties, these synthetic materials pose significant challenges and remain unclear in terms of biosafety [18,19]. Their use in coronary artery applications, for instance, could lead to undesirable side effects such as blood clotting or inflammation owing to their interaction with the bloodstream and biological tissues [6]. Furthermore, the complexity of the stimuli required to activate their shape memory response *in vivo* adds another layer of difficulty when translating these materials into practical clinical solutions.

To overcome these limitations, researchers have hypothesized that shape memory biopolymers based on naturally sourced materials could offer an easier and safer solution for biomedical applications [20,21]. Biopolymers, such as alginate, hyaluronic acid, gelatin, and chitosan, offer excellent biocompatibility, are highly renewable, and degrade safely within the body, reducing the risk of adverse reactions when used in medical devices [22–26]. These natural polymers can serve as an ideal foundation for creating blood-contacting devices such as bioresorbable stents, which require biocompatible and biodegradable materials, eliminating the need for surgical removal [14,15,27–29]. Their degradation over time can help reduce the burden of invasive procedures, making them highly suitable for the treatment of coronary artery disease.

Among these biopolymers, alginate stands out because of its ion-responsive properties, particularly its ability to form an “egg-box” structure when interacting with calcium ions [13,30]. This physical crosslinking creates a temporary gel state that can be reversed through ion exchange, thus endowing alginate with a unique shape memory capability [30]. However, alginate alone lacks the scaffolding network required to maintain a stable hydrogel structure under physiological conditions. To address this, a double-network hydrogel system can be employed by combining alginate with a second, more robust polymer network made from chemically crosslinked gelatin and chitosan [31]. This secondary network provides the structural integrity needed to maintain the hydrogel's form, whereas alginate facilitates shape memory behavior through ion interactions. This dual-network approach creates a hydrogel with two distinct states, fixed when the “egg-box” structure is intact and expanded when the ion crosslinking is disrupted, making it a promising material for biomedical applications.

In this study, we propose the use of a gelatin-chitosan-alginate-montmorillonite (GCAM) hydrogel as a shape memory material for biomedical applications. Alginate functions as an ion-responsive component, whereas gelatin and chitosan form a stable scaffold. Montmorillonite, a clay mineral, was incorporated to further enhance the mechanical properties and drug-carrying capacity of the hydrogel [14]. This paper outlines the preparation of a GCAM hydrogel, its shape memory properties, with a particular focus on its mechanical durability, biocompatibility, and drug-eluting capabilities. In addition to shape memory capability, this hydrogel exhibits self-healing behavior, controlled drug delivery, tissue adhesive characteristics, actuation potential, and electrical conductivity. Through *in vitro* studies, the swelling, degradation, and drug release behaviors of the hydrogel were evaluated, and the safety of the SMHs was assessed by incubating them with red blood cells and endothelial cells.

2. Materials and methods

2.1. Materials

Deacetylated chitosan from shrimp shells (CS, degree of deacetylation $\geq$ 75%), gelatin from porcine skin (GE, gel strength ~175 g Bloom, Type A), glutaraldehyde (GTA, 50 wt% in H_2O), glacial acetic acid (CH_3COOH, $\geq$ 99%), calcium chloride dihydrate ($CaCl_2{\cdot}2H_2O$, $\geq$ 99%), sodium bicarbonate ($NaHCO_3$, $\geq$ 99.7%) and phosphate buffered saline pH 7.4 (PBS) were obtained from Sigma-Aldrich Corporation (Missouri, United States). Montmorillonite (MMT) nanoparticles were kindly donated by Kunimine Industries Co., Ltd. (Tokyo, Japan). Alginic acid sodium salt from brown algae (SA) was provided by Duchefa Biochemie B.V. (Haarlem, The Netherlands). Enoxaparin sodium (Lovenox) was purchased from Sanofi S.A. (Paris, France). All the chemicals and solvents were used as received without further purification.

2.2. Characterization methods and statistical analysis

Fourier transform infrared spectroscopy (FTIR, ALPHA II, Bruker Corporation, USA) was used to identify the functional groups and characteristic linkages in the chemical structures of the SMHs. The spectra were measured in the range 4000–600 cm^{-1}. The morphological characteristics of the hydrogels were observed using scanning electron microscopy (SEM, JSM-6510, JEOL Ltd., Japan). ImageJ software (National Institutes of Health, United States) was used to determine pore size distribution from SEM images. The mechanical properties were evaluated by measuring the compression and tensile strengths. The compressive test was performed using a TA.XTplus Texture Analyzer (Stable Micro Systems Ltd., United Kingdom) at a constant rate of 1.0 mm/min, using cylindrical hydrogel samples. The compressive modulus was determined from the slope within the 5–15% strain range of the stress–strain curves. The tensile strength of the hydrogels was determined using a Universal Testing Machine M350-10 (The Testometric Company Ltd., United Kingdom) at a speed of 15.0 mm/min.

All data are presented as the mean $\pm$ standard deviation, and all experiments were performed in triplicate. Statistical evaluation of data was performed using the Student's *t*-test. Statistical significance was set at $p < 0.05$.

2.3. Preparation of SMHs

To develop the double-network structure, the primary polymer network forms via chemical crosslinking, whereas the secondary network is established temporarily through physical linkages. Specifically, a 3 wt% CS solution was prepared by dissolving in 1% acetic acid at 60 °C, and a 6 wt% GE solution was made by dissolving in deionized water (DIW) with stirring at 60 °C. MMT and SA were separately

dissolved in DIW at a concentration of 1 wt% each. The CS, GE, MMT, and SA solutions were then combined in a 30:20:1:0.75 vol ratio (v/v) under magnetic stirring to form a homogeneous mixture (100 mL). To form a primary network, a diluted 0.5 wt% GTA solution was added to this mixture in varying volumes (4 and 7 mL) and blended for 30 min. The resulting precursor solutions, designated GCAM4 and GCAM7, respectively, were poured into Petri dishes and allowed to react at 60 °C to facilitate the formation of chemically crosslinked GCAM hydrogels. A control gel without GTA, so called GCAM, was prepared using the same procedure. Scheme S1 shows the schematic illustration of the SMHs preparation process.

To examine the actuation property of the GCAM7 hydrogels, iron oxide nanoparticles were incorporated into the hydrogel in a site-specific manner. In brief, iron oxide nanoparticles were synthesized following our previous report [32]. Specifically, a defined volume of GCAM7 precursor solution was mixed with iron oxide nanoparticles (0.1 wt%) and then selectively injected into the desired region of the mold. This procedure generated a localized magnetic domain within the hydrogel, enabling region-specific actuation under an external magnetic field.

2.4. Swelling ratio

The swelling ratio of the GCAM samples was determined by measuring their weights before and after immersion in PBS. In brief, the dried samples were cut into small rectangular pieces and weighed to obtain the initial dry weight (W_0). The samples were then soaked in a container filled with PBS at 37 °C. At various time intervals (5, 10, 15, and 20 min), samples were removed from the fluid, gently blotted with filter paper, and swollen weights (W_t) were immediately measured. The swelling ratio was calculated using Eq. (1):

$$\text{Swelling ratio}\,(\%) = \frac{W_t - W_0}{W_0} \times 100\% \quad (1)$$

2.5. In vitro degradation

The rate of *in vitro* degradation of GCAMs was determined by measuring the weight loss of the hydrogels after immersion in a PBS solution at 37 °C in a water bath. The initial weight of hydrogels (W_0) were determined using a balance. At predetermined time intervals, the hydrogels were removed from the PBS solution, rinsed thoroughly with DIW, dried under vacuum, and reweighed (W_t). Weight loss was calculated as a percentage of the initial weight using Eq. (2):

$$\text{Weight loss}\,(\%) = \frac{W_0 - W_t}{W_0} \times 100\% \quad (2)$$

2.6. In vitro drug release

The release study was performed on enoxaparin-loaded hydrogels which were placed in a vial containing 10 mL of PBS solution (pH 7.4) at 37 °C. At predetermined time points, 2 mL of the release medium was collected and replaced with 2 mL of fresh PBS buffer solution. The amount of enoxaparin released was determined using a UV–Vis spectrophotometer (UV-1800, Shimadzu Corporation, Japan) based on a colorimetric Toluidine Blue O assay at an absorption wavelength of 530 nm. The cumulative release of enoxaparin was calculated using Eq. (3):

$$\text{Cumulative release}\,(\%) = \frac{V_0 \times C_t + V \times \sum_{n=1}^{t-1} C}{W} \times 100\% \quad (3)$$

where V_0 (mL) is the total volume of PBS used at the beginning of the experiment. V (mL) is the volume of the medium withdrawn at predetermined time. C_t (mg/mL) denotes the concentration of enoxaparin in the release medium at the specified time, while W (mg) refers to the weight of enoxaparin in the samples.

2.7. Shape memory behavior

The shape memory behavior of the GCAM hydrogels was evaluated by measuring the recovery ratio at room temperature. The GCAM7 samples with different shapes were prepared for shape memory testing. The temporary shape was then fixed by immersing the samples in a 3 wt % calcium solution. After removal from the calcium ion solution, the gels were immersed in a 10 wt% bicarbonate solution. The entire procedure was recorded using a digital camera. To assess the stability of the temporary shape, the hydrogel samples in their temporary state were immersed in 10 mM PBS (pH 7.4).

2.8. Self-healing behavior

The self-healing ability of GCAM hydrogels was visually demonstrated by coloring the samples with contrasting food dyes. Two differently colored hydrogels were gently placed in contact and allowed to stabilize for 1 h at room temperature. Photographs were obtained to document the self-healing process. In addition, the healed GCAM samples were evaluated by manual stretching and mechanical testing to assess their mechanical integrity.

2.9. Hemolysis test

The hemocompatibility of the hydrogels was assessed following established protocols [14]. Rabbit whole blood, anticoagulated with sodium citrate, was centrifuged at 3000 rpm for 15 min to isolate red blood cells (RBCs). The RBCs were rinsed twice with PBS to remove residual plasma and then diluted with PBS to obtain a 5% (v/v) RBC suspension. A suspension was prepared by adding diluted RBCs to a mixture of the hydrogel sample and PBS (pH 7.4) to achieve a final RBC concentration of 2% (v/v). Triton X-100 (1.0%) was used as a positive control, while PBS served as a negative control. The samples were incubated at 37 °C with mild shaking for 24 h, followed by centrifugation (3000 rpm for 15 min) to separate the supernatant. The absorbance of the supernatant was measured at 540 nm using a UV–Vis spectrophotometer, and the hemolysis ratio was calculated using Equation (4):

$$\text{Hemolysis ratio}\,(\%) = \frac{\text{OD}_{\text{sample}} - \text{OD}_{\text{negative}}}{\text{OD}_{\text{positive}} - \text{OD}_{\text{negative}}} \times 100\% \quad (4)$$

2.10. Chorioallantoic membrane assay

The biocompatibility of the hydrogels was evaluated using an *in ovo* chorioallantoic membrane (CAM) assay on chick embryos. On day 0, fertilized eggs were placed in an incubator at 37 °C and 55% humidity. On day 10 of incubation, the GCAM7 hydrogel was applied to the CAM of chick embryos. The eggs were covered with sterilized parafilm and secured with adhesive tape to maintain a sterile environment. On day 17, the eggs were opened and photographs of the hydrogel samples on the chick embryos were taken.

2.11. In vitro cell viability and live/dead cell imaging

For the cell viability test, mouse vascular endothelial cells (SVECs) were cultured in Dulbecco's modified Eagle's medium (DMEM) supplemented with 10% fetal bovine serum and 1% penicillin/streptomycin at 37 °C in a humidified atmosphere containing 5% CO_2. Cells were seeded in 96-well plates, with each well containing 100 μL of cell suspension at a density of 8×10^3 cells. Once attached, the cells were exposed to varying concentrations of the hydrogel and incubated at 37 °C for 24 h. After incubation, the medium was removed and cell viability was assessed using the MTT assay, a widely recognized method for this purpose. Optical density readings from the MTT assay provided insights into the cellular response to the hydrogel. Additionally, the LIVE/DEAD assay was conducted as a complementary approach to visually confirm

cell viability.

3. Results and discussion

3.1. Characterization of SMHs

The stacked FTIR spectra of the GCAM hydrogels are shown in Fig. 1A, including non-crosslinked GCAM and GCAM hydrogels crosslinked with GTA at various concentrations. The FTIR spectra of the GCAM samples reveal a broad trough around the wavenumber of 3262 cm^{-1}, indicative of O–H and N–H stretching vibrations associated with the functional groups in the polymeric components of the gel. Additionally, the absorption bands at 1537 and 1069 cm^{-1} correspond to N–H bending and C–O stretching, respectively [33]. In comparison with the non-crosslinked GCAM, crosslinked hydrogels exhibited a decreased transmittance band near 1633 cm^{-1}, which can be assigned to C═N stretching vibration associated with imine bond formation, overlapping with the C═O stretching vibration. These spectral changes confirmed the crosslinking of the GCAM gels by GTA.

Analysis of the XRD patterns of the pristine MMT and GCAM7 hydrogels provides valuable insights into their crystalline and amorphous states [34]. The XRD patterns of MMT and GCAM7 are shown in Fig. 1B. As expected, pristine MMT displayed prominent characteristic crystalline peaks at 6.9°, 14.1°, 18.8°, and 28.5° [35]. In contrast, the GCAM7 hydrogels showed broad peak at 22.1°, indicating the amorphous nature of the prepared GCAM7 hydrogel. The wide amorphous halo suggests that the biopolymers blended well. Notably, the characteristic MMT peak at 6.9° (2θ), corresponding to its basal (0 0 1) reflection, was no longer observed in the GCAM7 hydrogel. This disappearance suggests that the polymers were intercalated into the MMT galleries or even partially exfoliated, indicating that the layered structure of the nanoclay was largely disrupted and the clay platelets were well dispersed within the hydrogel matrix.

3.2. Surface properties

The surface and cross-sectional morphology of the GCAMs were analyzed using SEM. The morphology of the original GCAM7 top surface was distinctly different from its temporary form, likely because incubation in a calcium solution induced ionic crosslinking between SA chains, forming an “egg-box” structure and promoting gel network stabilization. Interestingly, when temporarily fixed GCAM7 were subsequently incubated with bicarbonate ions, it returned to its original shape, as confirmed by smooth surface property (Fig. 1C).

3.3. Swelling ratio

The swelling ratio is a crucial parameter in the application of hydrogels in biomedical fields, as it determines their ability to absorb fluids and exchange nutrients and waste [36]. The swelling capacity and stiffness of hydrogels are influenced by hydrophilicity, polymer interactions, and crosslink density. Fig. 2A and B show the swelling ratios of the hydrogels. All three GCAM gels nearly reached a plateau within 20 min, indicating their high hydrophilicity and rapid swelling in aqueous environments. Furthermore, hydrogels containing crosslinkers exhibited greater swelling compared to those without crosslinkers, with swelling increasing as GTA content increased (285.4 ± 3.4% and 324.1 ± 22.4%, respectively). As shown in Fig. 2A, the non-crosslinked GCAM hydrogel began to exhibit minimal cracking after 5 min, which progressed to significant rupture after 20 min. In contrast, the other two

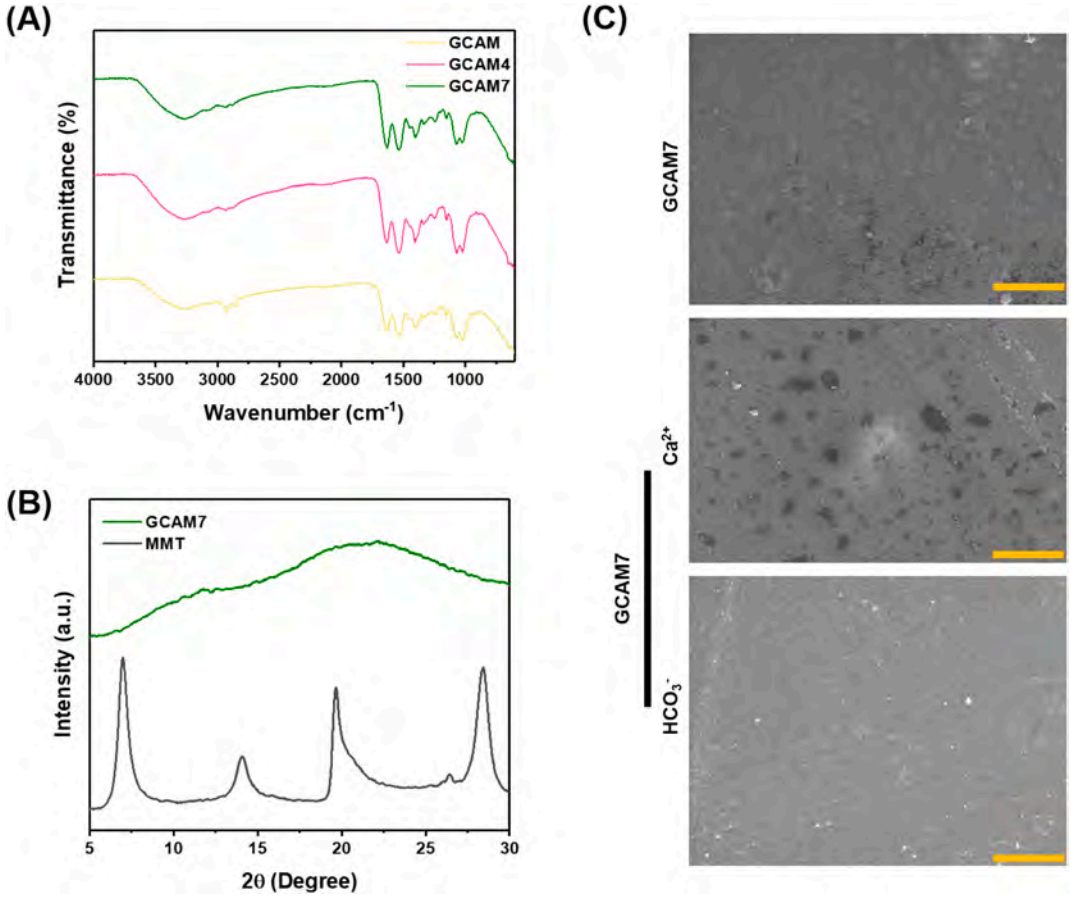

Fig. 1. (A) FTIR spectra of GCAM hydrogels. (B) XRD spectra of GCAM7 and MMT. (C) Surface properties of the GCAM7 hydrogels were investigated using SEM. Calcium and bicarbonate ions were used to fix the temporary shape and trigger the shape recovery of the GCAM7. Scale bar: 20 μm.

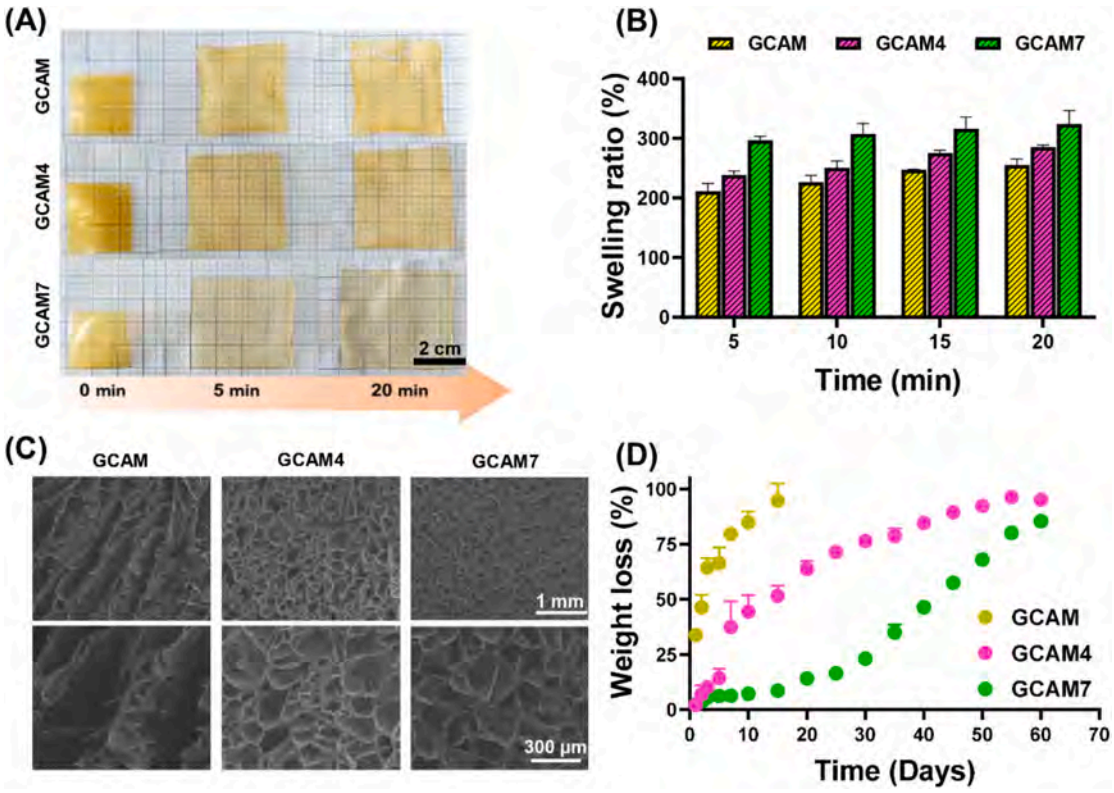

Fig. 2. Swelling behavior of SMHs. (A) Swelling photographs of the different GCAM hydrogels as a function of time. (B) Swelling ratio graph of GCAM hydrogels. (C) SEM images of swollen GCAM hydrogels. (D) *In vitro* degradation study of the GCAM hydrogels.

samples (GCAM4 and GCAM7), which contained crosslinkers, maintained their shape and structural integrity without bending or cracking. The abundant amine and hydroxyl groups on the GE and CS backbones create highly probable sites for strong water affinity [37]. In the crosslinked samples, GTA crosslinked with other components decreased the number of functionalities and established a firm three-dimensional framework, which increased the stability and endurance of the hydrogels towards swelling response. Moreover, a higher swelling ratio indicates a better absorption capacity [38]. Regarding the shape change performance, this feature provides hydrogels with interesting properties, as they can ingest a large volume of liquid and expand their size quickly when soaked in an aqueous environment, which in turn supplements a repulsion force for the enlargement of the shape memory hydrogel.

Fig. 2C illustrates the cross-sectional morphology of the GCAM hydrogels swollen in PBS, highlighting the expansion of the pore volume and its dependence on crosslinking ratio. SEM images revealed that all hydrogels exhibited a porous sponge-like structure. Notably, the crosslinked hydrogels exhibited a more homogeneous and intact pore architecture, in contrast to the uneven and fractured pores observed in the non-crosslinked sample.

Water retention capacity is influenced by several factors, including hydrophilic groups, chain flexibility, crosslinking density, and structural integrity. When a hydrogel absorbs water and swells, internal forces develop in the gel network. If the network cannot withstand these forces, water diffuses out. However, with sufficient crosslinking, the gel retained water within its structure. This mechanism likely explains the trend observed among the hydrogels. Additionally, the inclusion of crosslinkers improved the mechanical properties of the hydrogels, providing greater structural stability and resistance to pore deformation in the swollen state.

3.4. *In vitro degradation*

Hydrolytic degradation is an essential consideration for the use of hydrogels in biomedical applications. This process involves the breakdown of hydrogel polymer chains through hydrolysis [39]. Hydrolytic degradation is a desirable feature for some applications, as it can lead to the controlled release of encapsulated drugs or growth factors or the gradual erosion of the hydrogel matrix to facilitate tissue regeneration [40]. In addition, it can reveal a limitation in the long-term stability of the hydrogels. Fig. 2D shows the weight loss curve of the shape memory hydrogels after 60 days of incubation in PBS (pH 7.4) at 37 °C. Under these conditions, an initial weight loss due to the degradation of the GCAM hydrogels was observed. The hydrogels exhibited a gradual deterioration rate, starting in the first week. Notably, GCAM4 and GCAM7 showed slower degradation than GCAM hydrogels. It is noteworthy that GCAM7 showed only around 14.1 ± 0.3% weight loss on day 20. This suggests that an increase in the crosslinking density controlled hydrogel degradation, which agrees with previously reported crosslinked hydrogels [41,42]. Subsequently, a notable increase in the *in vitro* degradation rate was observed in GCAM7, with a weight loss of 85.4 ± 2.1% by day 60. Although the degradation rate of the gel increased significantly over time, GCAM7 still exhibited excellent stability and biodegradability for biomedical applications. The enhanced stability of GCAM7 is attributed to the inter- and intramolecular crosslinking between CS and GE [43,44]. This combination leverages the biocompatibility of both polymers while optimizing their mechanical properties and degradation rates. Additionally, the reinforcement of MMT likely contributed to the stability of the hydrogel under *in vitro* conditions.

3.5. *Mechanical properties*

To understand how crosslinking affects the mechanical behavior of the hydrogel, we measured the compression property of GCAMs, as

shown in Fig. S1. According to the compression test results, all GCAM hydrogels exhibited large deformations under low stress, demonstrating soft tissue-like properties. Additionally, as the concentration of the crosslinker increased, a low modulus was maintained up to 70% strain without failure. This result highlighted the hydrogel's high water retention capacity and its ability to crosslink and build up a stable network structure. These findings are consistent with the results of the investigation of the swelling properties. This indicates a clear correlation between the crosslinking density and the mechanical properties of the system. The crosslinking density needs to be sufficient to enhance the hydrogel's stability; however, an excessively high crosslinking density may reduce the flexibility of polymer chains, impairing the material's ability to absorb and distribute stress, which ultimately makes the hydrogel more brittle [45,46].

3.6. Self-healing behavior

The self-healing behavior of hydrogels is a highly desirable property that can extend their practical applications across multiple domains [47–49]. In this study, we examined the self-healing behavior of a GCAM hydrogel and found that it displayed outstanding self-healing properties (Fig. 3Ai and Fig. S2). GCAM hydrogels stained in different colors seamlessly re-adhered and healed rapidly upon contact at room temperature for 1 h, highlighting their excellent self-healing properties. Magnified images indicated a color-blended section at the contact surface, demonstrating the self-healing performance of the different hydrogel pieces. Hydrogen bonding interaction and dynamic covalent imine bonds play a critical role in the self-healing process, whereas residual functional groups in the matrices strengthen the binding dynamics, facilitating the re-adhesion and healing [45].

To validate the restoration of the original mechanical properties of the hydrogel, we manually assessed the strength of the healed hydrogels after re-adhesion (Fig. 3Aii). This assessment involved applying lifting, stretching along longitudinal axis of the testing specimens. The gel retained its stability, exhibiting no signs of fracturing over time. Interestingly, upon manual stretching, the gel demonstrated exceptional elasticity without breaking at the scar section, thereby confirming the robust self-healing behavior of the GCAM system (Fig. S2B). To further explore the exceptional flexibility and self-healing capabilities of GCAMs, hydrogel blocks stained with different colors were arranged alternately and brought into contact to initiate self-healing (Fig. S2A). After healing, the GCAM row forms a cohesive structure in tandem. When pulled horizontally, the self-healing row demonstrated remarkable structural integrity.

The SMH developed by our group also demonstrated enhanced properties, such as electrical conductivity and flexible wearability. The

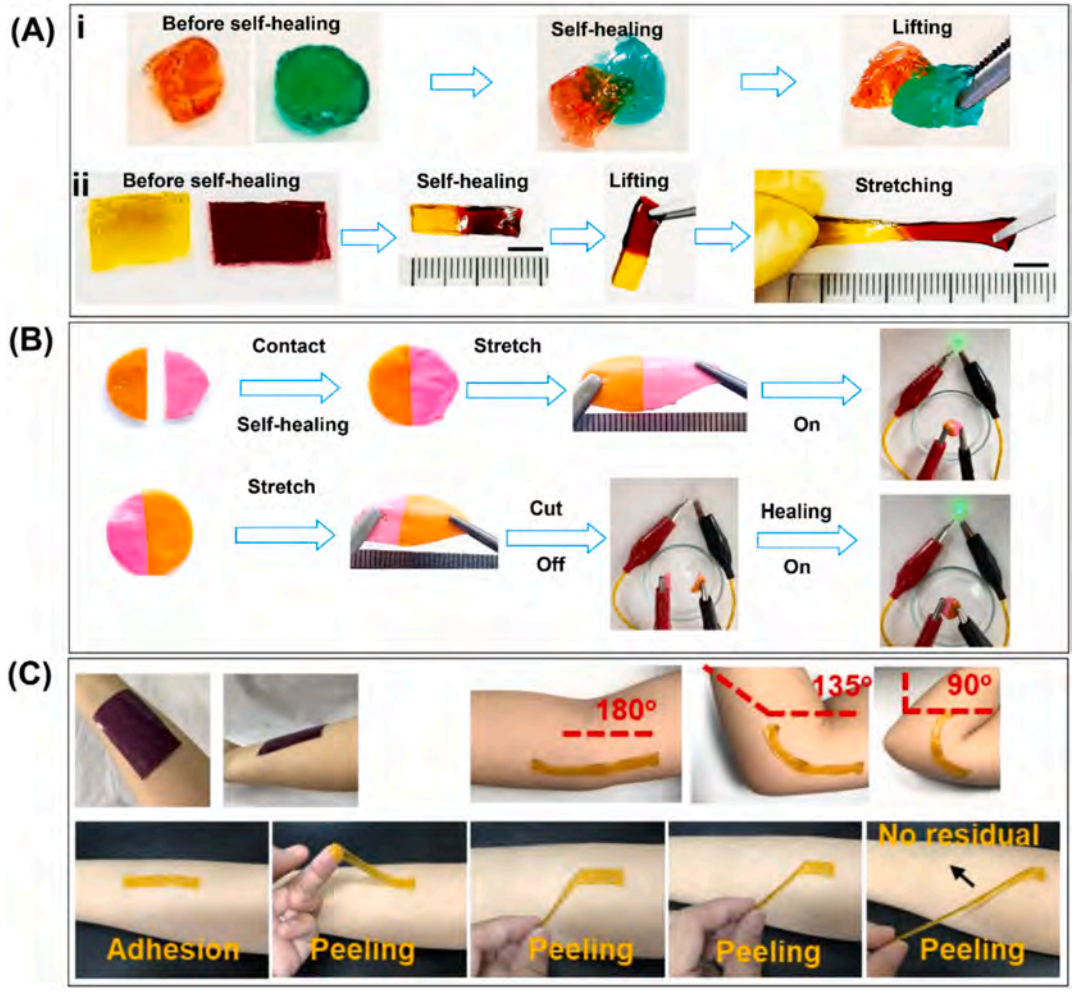

Fig. 3. Self-healing properties of GCAM hydrogels. (A) Photographs showing self-healing in GCAM hydrogels of different colors and shapes, including sphere and strip forms. When placed in close contact, the hydrogels spontaneously self-healed after 1 h, demonstrating the effective interactions between the sections. The healed hydrogels withstood stretching, thereby highlighting their flexibility and mechanical strength. (B) Real-time conductivity measurements of self-healing GCAM hydrogels. (C) Adhesion performance of GCAM hydrogels on human skin and elbow during exercise. The hydrogels adhered securely but peeled off cleanly, leaving no residues on the skin.

incorporation of these attributes has broadened the application potential of the GCAM system. As shown in Fig. 3B, two differently colored GCAM samples were initially separated; however, after a physical contact for a short period (30 min), they displayed self-bonding. The bonding strength was confirmed through a tweezer test, which revealed that the fused hydrogel samples held together robustly. To validate the functional recovery of the material, we set up a conductivity test using a power source and a light bulb. The results showed that the light bulb was illuminated, indicating that the GCAM hydrogel reconnected after the self-healing process, thereby completing the circuit. In contrast, cutting the healed hydrogel in half broke the circuit and the light went out and vice versa.

Additionally, we evaluated the adhesion properties of the GCAM hydrogel when applied to the human skin (Fig. 3C). The hydrogel sample exhibited excellent adhesion and elasticity, conforming well to arm movement. After being completely peeled off, no residue remained, highlighting its durability and convenience for skin applications. Our results suggest that this hydrogel has tremendous potential for various applications, including drug delivery, motion sensors, and tissue engineering.

3.7. Mechanical and electrical properties

To further elucidate the robustness of the self-healing function, the mechanical and electrical properties of GCAM7 were evaluated before and after healing. A quantitative assessment of self-healed SMHs based on tensile tests comparing the mechanical properties of the original and self-healed GCAM7 hydrogels was shown in Fig. 4. The pristine hydrogel exhibited a fracture stress of 232 kPa, whereas the healed sample (after 1 h of autonomous healing) reached 210 kPa before breaking. The high retention of tensile strength demonstrates that the hydrogel effectively reconstructed its load-bearing polymer network following mechanical damage, which is attributed to the dynamic and reversible bonds within the hydrogel matrix that allow the fracture to reconnect and restore mechanical integrity. The self-healed samples retained approximately 90% of the original tensile strength and 58% of the original fracture strain, demonstrating effective recovery of mechanical integrity after damage (Fig. 4A–C). Furthermore, electrical conductivity of the GCAM7 hydrogels before and after self-healing, we performed quantitative electrical conductivity measurements using a standard two-probe setup [50]. These measurements further confirmed the functional recovery of the GCAM7 hydrogel after self-healing. The original, undamaged hydrogel showed a conductivity of 0.165 S/m, whereas the self-healed sample exhibited a conductivity of 0.155 S/m (Fig. 4D, Fig. S3). This result demonstrates that the reconstructed network effectively restores conductive pathways, enabling stable electrical performance even after mechanical damage.

As shown in the SEM micrographs (Fig. S4), the boundary between the two previously separated fragments is no longer visible after healing, and the porous network becomes fully continuous across the interface. This morphological continuity indicated that polymer chains from both sides interpenetrated and reconstructed the microstructure following damage, providing visual evidence for the proposed self-healing mechanism. Together, these mechanical, electrical, and morphological results demonstrated that GCAM7 can effectively recover a continuous, functional network after damage, supporting its use in reusable or long-lasting soft devices.

3.8. Shape memory behavior

The shape memory behavior of hydrogels has gained significant interest in biomedical applications owing to its ability to mimic natural tissue deformation and recover its original shape. In this study, we demonstrated the shape memory behavior of hydrogels of various shapes. First, we evaluated the shape memory behavior of the stent-like shaped crosslinked GCAM and found that it exhibited satisfactory shape

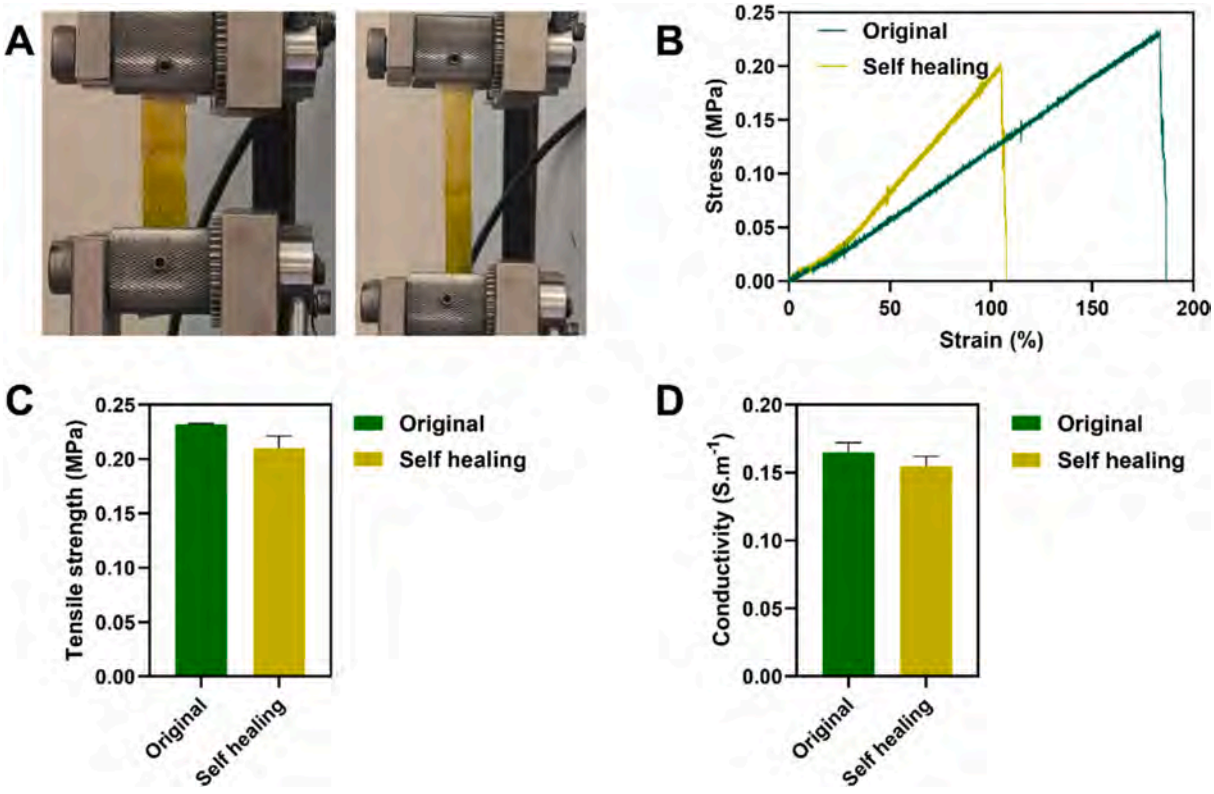

Fig. 4. Mechanical and electrical properties of self-healed GCAM7 hydrogels. (A) Photographs showing tensile testing of self-healed samples. (B) Stress–strain curves of pristine and self-healed hydrogels. (C) Tensile strength of original and healed samples, indicating high retention of mechanical properties after 1 h of self-healing. (D) Electrical conductivity of original and healed hydrogels, showing minimal loss of conductivity after healing.

memory behavior (Fig. 5A). The shape memory property of stents is crucial for biomedical applications because it enables the stent to adapt to the shape of the blood vessel, leading to a better treatment outcome (Scheme S2). In conclusion, our study highlights the potential of hydrogels for developing innovative stents for biomedical applications, thereby contributing to the advancement of biomedical engineering.

To further evaluate the shape memory properties of the GCAMs, hydrogels with various shapes (ring, flowers, star, and umbrella) were prepared, and their shape recovery behavior was examined (Fig. 5B, C, and D). For instance, the original flower-like hydrogel was folded into a tight square and fixed in a 3 wt% calcium solution to obtain a temporary morphology. Here, the alginate chains complexed with calcium cations, where they were sandwiched between two alginate molecules to form an "egg-box" structure, inducing calcium alginate gelation and retaining the temporary shape. Subsequently, the square hydrogel was transferred to 10 wt% bicarbonate solution at room temperature, where ion exchange weakened the calcium ion–alginate coordination and disrupted the "egg-box" structure. As a result, the hydrogel rapidly lost its square

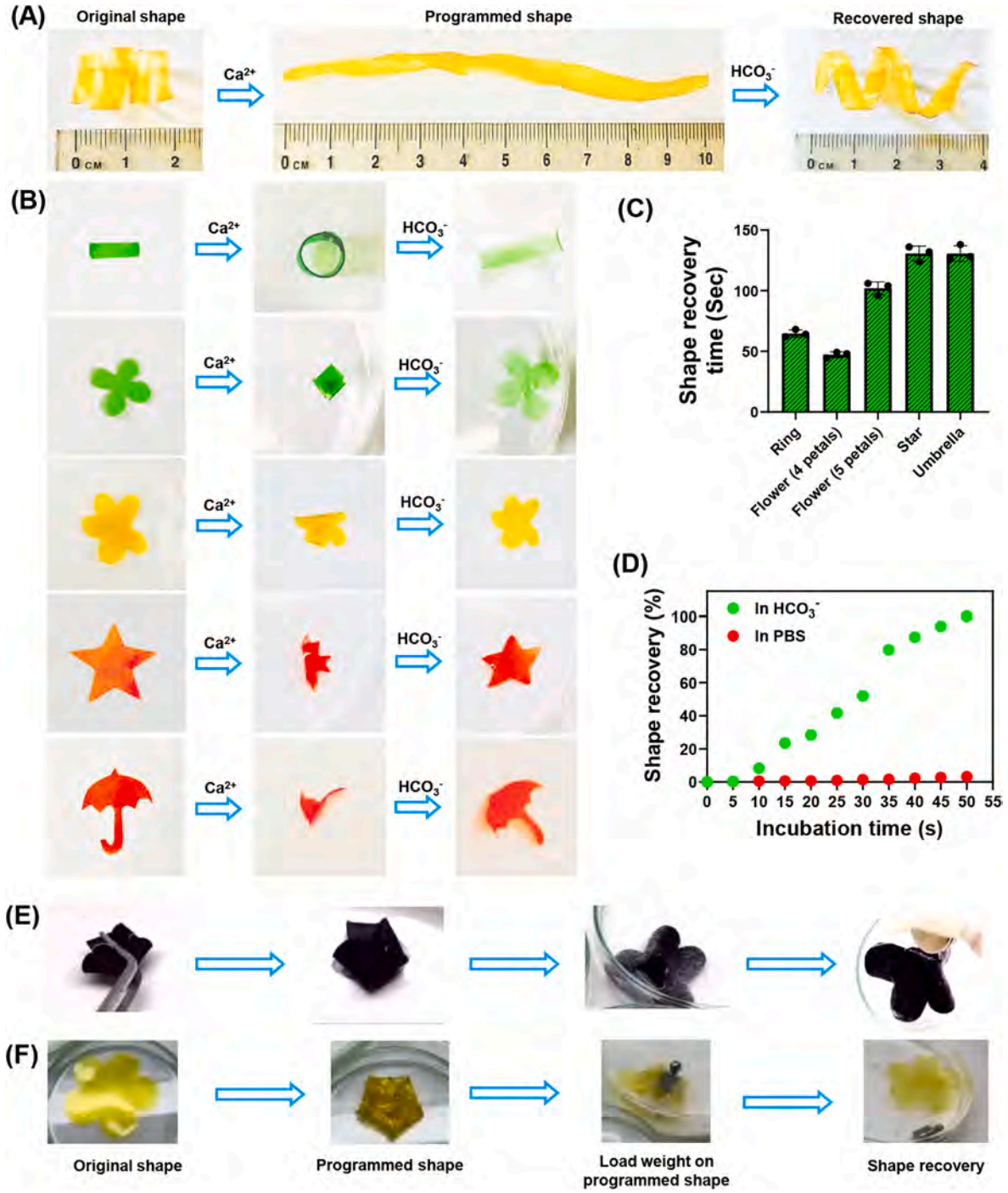

Fig. 5. Shape memory performance of GCAMs. (A) Stent-like shaped sample. (B) The prepared GCAMs samples with different shapes. The specimens were programmed to temporary shape by immersing in a 3 wt% calcium ion solution. The temporary shape was then removed and immersed in a 10 wt% bicarbonate solution to restore its original shape. (C) Shape recovery times for different shapes. (D) Time-dependent shape recovery of six-petal flower-shaped GCAM7 hydrogels in different buffer solutions. (E) Shape memory and actuation properties of the GCAM hydrogels. Site-specific programming of a single petal enables actuation in response to a magnet. (F) Shape memory and recovery of GCAM hydrogels after placing 10 g load.

shape and recovered its original configuration.

To illustrate the shape memory capability of the hydrogel sample, a schematic illustration of the temporary crosslinking and shape-recovery mechanisms of the SMHs is shown in Scheme 1. When GCAM, initially fixed in shape using calcium ions, an “egg-box” structure forms, establishing a secondary crosslinked network following GTA crosslinking. This temporary network stabilizes the shape of the hydrogel. Upon immersion in a $NaHCO_3$ solution, bicarbonate ions have a strong affinity for calcium, forming $Ca(HCO_3)_2$, which may further convert to $CaCO_3$ precipitates, disrupting the "egg-box" structure, allowing the hydrogels to recover their original shapes.

Actuation experiments were conducted to evaluate the potential of the GCAMs as soft magnetic actuators. As depicted in Fig. 5E, a flower-shaped hydrogel with five petals was prepared, with iron oxide nanoparticles site-specifically loaded on one side of each petal, whereas the other side remained nanoparticle-free. When a magnet was brought close to the hydrogel, the nanoparticle-loaded sides of the petals exhibited strong attraction, demonstrating the soft magnetic actuation capabilities of the material.

To confirm the robust physical and mechanical properties of these shape memory materials, additional experiments were performed under weight-restrained recovery conditions. Interestingly, the hydrogel recovered its shape when subjected to a moderate weight of 10 g, as shown in Fig. 5F. The result highlights the remarkable ion-responsive shape memory behavior, underscoring its potential for applications such as biodegradable stents.

3.9. Shape memory behavior in different buffer solutions

To elucidate the ion-responsive shape memory behavior of GCAM7, shape fixity and recovery were evaluated for a six-petal flower-shaped sample in different solutions. The shape fixity ratio and shape recovery ratio were determined by monitoring changes in the projected area during the fixing and unfolding processes. The sample exhibited an excellent shape fixity ratio of approximately 100% and showed rapid shape recovery in 10 wt% bicarbonate solution, achieving about 52% recovery at ~30 s, over 90% recovery at 45 s, and nearly complete recovery to its original shape at 50 s (Fig. S5). In contrast, when the calcium ion-programmed hydrogel was immersed in PBS, no shape recovery was observed, and the temporary configuration was fully retained over the entire observation period.

3.10. Drug release studies

The dual-network structure in the GCAM hydrogels was hypothesized to enable sustained release of the therapeutic agent. Enoxaparin, a commonly used anticoagulant for preventing thrombosis and clot formation in stents, was encapsulated in the hydrogels. The release profiles of the GCAM hydrogels showed sustained release of enoxaparin (Fig. 6A). In particular, the extent of drug release depended on the hydrogel crosslinking ratio. GCAM without any crosslinking exhibited a somewhat faster drug release compared to the crosslinked formulations, GCAM4 and GCAM7. As expected, GCAM7 demonstrated a more sustained release profile than other formulations, with a cumulative release of 91.6 ± 5.4% after 14 days.

Release kinetic models were applied to all three hydrogel samples to investigate the drug release mechanisms (Table S1). The kinetic analysis revealed that the release profiles for all three hydrogels were best fitted to the zero-order kinetic model. This indicates that the enoxaparin was released at a nearly constant and continuous rate over a defined period, independent of the total amount of the drug remaining. Furthermore, utilizing the Korsmeyer–Peppas model, the regression exponent n for the GCAM sample corresponded to a value of 0.37, suggesting that the primary driving force of the release process was diffusion. Meanwhile, the GCAM4 sample, with an n value of 0.51, indicated the onset of a hybrid mechanism involving polymer chain relaxation. However, as the crosslinking density increased, this hybridity appeared to diminish. The emergence of this hybrid mechanism in the release process aligns with the extension of polymer chains in solution, as evidenced by the swelling ratio results of GCAM4 and GCAM7 relative to GCAM. For GCAM7, the combination of higher crosslinking density and a more uniform porous structure implies that polymer chain relaxation is no longer the dominant contributor to release; instead, the stable pore network provides pathways that are more favorable for diffusion-controlled transport.

3.11. Hemolysis assay

Hemocompatibility is crucial for the safe use of biomaterials that come in contact with blood, and the *in vitro* hemolysis assay is the most common method to evaluate hemocompatibility. As shown in Fig. 6B, the vial containing GCAM7 displayed a color similar to the negative control, whereas the positive control presented a bright red color, indicating hemolytic activity. The GCAM7 hydrogel exhibited a hemolysis ratio of less than 3%, indicating good hemocompatibility. This finding supports the potential of the hydrogel as a safe material for

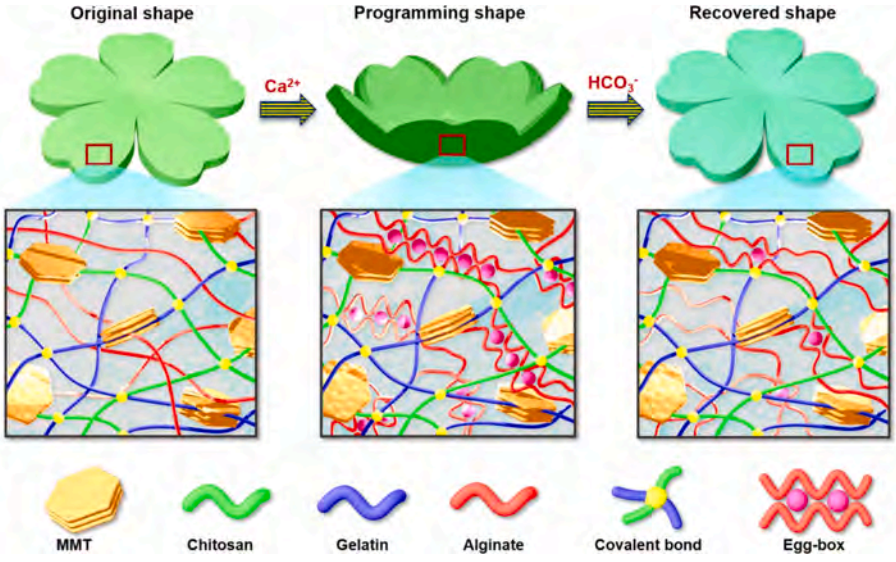

Scheme 1. Schematic illustration of temporary crosslinking and shape recovery mechanisms of SMHs.

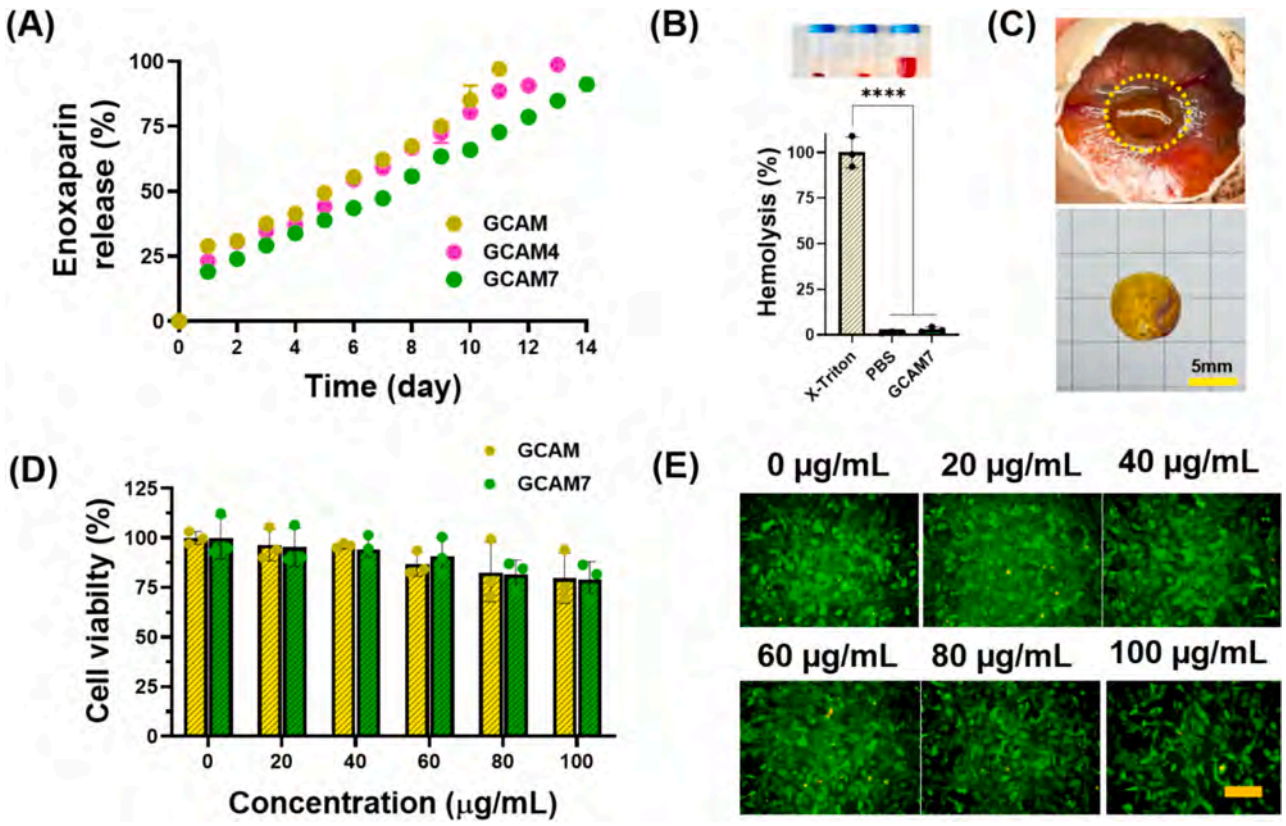

Fig. 6. *In vitro* studies of GCAMs. (A) Cumulative enoxaparin release from the GCAM hydrogels. (B) Hemolytic activity of GCAM and visualized photographs of the hemolysis assay. (C) Hydrogel placed on CAM recovered after 7 days. (D and E) Viability and LIVE/DEAD assay of SVECs treated with GCAM (scale bar: 50 μm).

biomedical applications, especially for blood-contacting purposes.

3.12. CAM assay

The CAM assay is a valuable tool for assessing biocompatibility and potential therapeutic effects of novel biomaterials, particularly those intended for use in tissue engineering and regenerative medicine. The CAM assay was performed by implanting the materials onto the chorioallantoic membrane and monitoring chick embryo health and survival, as well as changes in vascularization surrounding the implantation site. Preliminary result indicated that the hydrogel did not induce obvious anomalies or inflammation at the implantation site (Fig. 6C), suggesting acceptable biocompatibility under the tested conditions.

3.13. Biocompatibility of GCAMs on SVECs

Our research focused on biosafety evaluation of the GCAM hydrogel, specifically its biocompatibility, which is essential because of its direct contact with damaged vessels and injured tissues. We used to simulate cellular interactions that are typical of clinical applications. As shown in Fig. 6D, a slight decline in cell survival was observed when cells were cultured with varying hydrogel concentrations. Notably, SVECs showed a gradual reduction in viability as the GCAM hydrogel concentration increased. However, even at 80 μg/mL, SVECs maintained viability above 80%, demonstrating considerable biocompatibility. The LIVE/DEAD assay results further supported these findings, showing minimal cell death across different concentrations and cell types as well as healthy cellular proliferation (Fig. 6E).

After establishing the individual physicochemical and biological properties of the shape memory hydrogels, we next integrated these metrics into a comparative radar plot that benchmarks our GCAM7 hydrogel against representative recently reported systems, enabling a concise visualization of its overall performance advantage [51–54] (Fig. S6). Across six normalized metrics, including shape fixity, final shape recovery ratio, recovery time, tensile strength, self-healing efficiency, and adhesive strength or electrical conductivity, GCAM7 occupies a larger area than the reference systems, indicating a more balanced combination of rapid and nearly complete shape recovery, robust mechanics, and additional functional properties. This integrated comparison highlights the competitive advantages of GCAM7 as a versatile hydrogel platform. Literature systems often prioritize one or two functions, such as high toughness, strong tissue adhesion, or electrical conductivity, but typically exhibit slower recovery, limited programmability, or rely on synthetic matrices and complex chemistries. In contrast, GCAM7 achieves nearly complete shape recovery within tens of seconds even for complex flower-like geometries, maintains high tensile strength and electrical conductivity after self-healing, and adheres strongly to wet tissues. This integrated balance of speed, stability, and multifunctionality suggests that GCAM7 is particularly well suited for minimally invasive, bioresorbable devices where reliable actuation, structural endurance, and local therapeutic functions must operate simultaneously.

4. Conclusions

In summary, we successfully developed a novel SMH using natural materials, including chitosan, gelatin, alginic acid, and montmorillonite, which showed exceptional multifunctionality for biomedical applications. The SMH demonstrated outstanding shape-shifting capabilities, which could be precisely tuned by modulating environmental ion concentrations under physiological conditions. With rapid shape fixation and recovery, the hydrogel proved to be highly versatile for dynamic and responsive applications. The reversible functional properties of the hydrogel after self-healing highlight its durability and adaptability,

ensuring prolonged usability in demanding biomedical environments. Additionally, the material exhibited excellent biocompatibility, biodegradability, and sustained drug release capabilities. These synergistic attributes make SMH an excellent candidate for advanced biomedical applications. By combining tunable mechanical properties, sustained therapeutic efficacy, and biocompatibility, this study lays a strong foundation for the development of next generation hydrogel-based solutions in regenerative medicine and therapeutic interventions.

CRediT authorship contribution statement

Ha Huong: Writing – original draft, Visualization, Investigation, Formal analysis, Data curation, Conceptualization. **Cuong Hung Luu:** Writing – original draft, Visualization, Investigation, Formal analysis, Data curation, Conceptualization. **V.H. Giang Phan:** Writing – original draft, Visualization, Investigation, Formal analysis, Data curation, Conceptualization. **Gopinathan Janarthanan:** Visualization, Investigation, Formal analysis, Data curation, Conceptualization. **Ngoc-Thuy Huynh:** Validation, Investigation, Data curation. **Hieu Trung Nguyen:** Validation, Investigation, Data curation. **Nhu-Y Ngoc Ha:** Validation, Investigation, Data curation. **Hang Thu Ta:** Writing – review & editing, Supervision, Investigation, Conceptualization. **Qihui Zhou:** Writing – review & editing, Supervision, Investigation, Conceptualization. **Sanjairaj Vijayavenkataraman:** Writing – review & editing, Supervision, Investigation, Conceptualization. **João Conde:** Writing – review & editing, Supervision, Investigation, Funding acquisition, Conceptualization. **Thavasyappan Thambi:** Writing – review & editing, Supervision, Investigation, Funding acquisition, Conceptualization.

Declaration of competing interest

The authors declare the following financial interests/personal relationships which may be considered as potential competing interests: J. C. is a co-founder and shareholder of TargTex S.A. – Targeted therapeutics for Glioblastoma Multiforme. J.C. is a member of the Global Burden Disease (GBD) consortium of the Institute for Health Metrics and Evaluation (IHME), University of Washington (US) and is on the Scientific Advisory board of Vector Bioscience Cambridge. The other authors have no conflicts of interest to declare.

Acknowledgements

J.C. acknowledges the Fundação Ciência e Tecnologia, IP national support, through CHRC (04923/2020) and the FCT Grant LISBOA2030-FEDER-00862500-14998. This work was supported by the National Research Foundation of Korea (NRF) grant funded by the Korea government (MSIT) (NRF-2023R1A2C1005904). This work was also supported by the Queensland node of the Australian National Fabrication Facility, Griffith University (ANFF) and Qingdao Key Technology Research and Industrialization Demonstration Project (25-1-1-gjgg-66-nsh). This work was also supported by Ton Duc Thang University.

Appendix A. Supplementary data

Supplementary data to this article can be found online at https://doi.org/10.1016/j.matdes.2026.115736.

Data availability

The data that support the findings of this study are available from the corresponding author upon reasonable request.

References

[1] W.A. Brantley, Evolution, clinical applications, and prospects of nickel-titanium alloys for orthodontic purposes, J. World Federat. Orthodontists 9 (3 Supplement) (2020) S19–S26.
[2] Y. Liang, L. Yue, Evolution and development: engine-driven endodontic rotary nickel-titanium instruments, Int. J. Oral Sci. 14 (1) (2022) 12.
[3] N. Lokesh, U.S. Mallikarjun, A.G. Shivasiddaramaiah, Synthesis and evaluation of shape memory effect of Cu-Al-Ni shape memory alloys, AIP Conf. Proc. 2274 (1) (2020).
[4] H. Holman, M.N. Kavarana, T.K. Rajab, Smart materials in cardiovascular implants: Shape memory alloys and shape memory polymers, Artif. Organs 45 (5) (2021) 454–463.
[5] M. Balasubramanian, R. Srimath, L. Vignesh, S. Rajesh, Application of shape memory alloys in engineering – a review, J. Phys. Conf. Ser. 2054 (1) (2021) 012078.
[6] C.H. Luu, N.-T. Nguyen, H.T. Ta, Unravelling surface modification strategies for preventing medical device-induced thrombosis, Adv. Healthc. Mater. 13 (1) (2024) 2301039.
[7] A. Biesiekierski, J. Wang, M. Abdel-Hady Gepreel, C. Wen, A new look at biomedical Ti-based shape memory alloys, Acta Biomater. 8 (5) (2012) 1661–1669.
[8] J. Shang, X. Le, J. Zhang, T. Chen, P. Theato, Trends in polymeric shape memory hydrogels and hydrogel actuators, Polym. Chem. 10 (9) (2019) 1036–1055.
[9] C. Löwenberg, M. Balk, C. Wischke, M. Behl, A. Lendlein, Shape-memory hydrogels: evolution of structural principles to enable shape switching of hydrophilic polymer networks, Acc. Chem. Res. 50 (4) (2017) 723–732.
[10] D.C.S. Costa, P.D.C. Costa, M.C. Gomes, A. Chandrakar, P.A. Wieringa, L. Moroni, J.F. Mano, Universal strategy for designing shape memory hydrogels, ACS Mater. Lett. 4 (4) (2022) 701–706.
[11] B. Aaliya, K.V. Sunooj, M. Lackner, Biopolymer composites: a review, Int. J. Biobased Plast. 3 (1) (2021) 40–84.
[12] V.H.G. Phan, M. Murugesan, P.P.T. Nguyen, C.H. Luu, N.-H.-H. Le, H.T. Nguyen, P. Manivasagan, E.-S. Jang, Y. Li, T. Thambi, Biomimetic injectable hydrogel based on silk fibroin/hyaluronic acid embedded with methylprednisolone for cartilage regeneration, Colloids Surf. B Biointerfaces 219 (2022) 112859.
[13] C.H. Luu, G. Nguyen, T.-T. Le, T.-M.-N. Nguyen, V.H. Giang Phan, M. Murugesan, R. Mathiyalagan, L. Jing, G. Janarthanan, D.C. Yang, Y. Li, T. Thambi, Graphene oxide-reinforced alginate hydrogel for controlled release of local anesthetics: synthesis, characterization, and release studies, Gels 8 (4) (2022) 246.
[14] P.-K.-T. Ngo, D.N. Nguyen, H.-P. Nguyen, T.-H.-H. Tran, Q.-N.-D. Nguyen, C. H. Luu, T.-H. Phan, P.K. Le, V.H.G. Phan, H.T. Ta, T. Thambi, Silk fibroin/chitosan/montmorillonite sponge dressing: enhancing hemostasis, antimicrobial activity, and angiogenesis for advanced wound healing applications, Int. J. Biol. Macromol. 279 (2024) 135329.
[15] Y. Xia, Y. He, F. Zhang, Y. Liu, J. Leng, A review of shape memory polymers and composites: mechanisms, materials, and applications, Adv. Mater. 33 (6) (2021) 2000713.
[16] A. Naeem, C. Yu, L. Zhou, Y. Xie, Y. Weng, Y. Huang, M. Zhang, Q. Yang, Shape memory hydrogels in tissue engineering: recent advances and challenges, Bioact. Mater. 54 (2025) 215–247.
[17] C. Lin, M. Yang, F. Zhang, Y. Liu, J. Leng, Stimuli-responsive smart materials for biomedical applications, Mater. Sci. Eng.: R: Rep. 167 (2026) 101126.
[18] S. Lanzalaco, J. Mingot, J. Torras, C. Alemán, E. Armelin, Recent advances in poly (N-isopropylacrylamide) hydrogels and derivatives as promising materials for biomedical and engineering emerging applications, Adv. Eng. Mater. 25 (4) (2023) 2201303.
[19] F. Zhou, L. Qi, X. He, Synergistic toughening of iso-polypropylene with high-density polyethylene and polycyclooctene synthesized by ROMP, Polym. Adv. Technol. 31 (11) (2020) 2492–2503.
[20] Y. Cui, D. Li, C. Gong, C. Chang, Bioinspired shape memory hydrogel artificial muscles driven by solvents, ACS Nano 15 (8) (2021) 13712–13720.
[21] S. Yang, Y. Zhang, T. Wang, W. Sun, Z. Tong, Ultrafast and programmable shape memory hydrogel of gelatin soaked in tannic acid solution, ACS Appl. Mater. Interfaces 12 (41) (2020) 46701–46709.
[22] M. Li, H. Qu, Q. Li, S. Lu, Y. Wu, Z. Tang, X. Liu, Z. Yuan, L. Huang, L. Chen, H. Wu, A carboxymethyl cellulose/chitosan-based hydrogel harvests robust adhesive, on-demand detachment and self-healing performances for deep burn healing, Chem. Eng. J. 498 (2024) 155552.
[23] X. Liu, L. Chen, A. Sufu, F. Liu, Stretchable and self-healing carboxymethyl cellulose/polyacrylic acid conductive hydrogels for monitoring human motions and electrophysiological signals, Int. J. Biol. Macromol. 293 (2025) 138900.
[24] C.M. Phan, C.H. Luu, M. Murugesan, T.-N.-Q. Nguyen, N.-Y.-N. Ha, H.L. Ngo, N.-D.-H. Nguyen, Z. Pan, V.H.G. Phan, Y. Li, T. Thambi, Injectable gelatin-pectin hydrogel for dental tissue engineering: enhanced angiogenesis and antibacterial efficacy for pulpitis therapy, Int. J. Biol. Macromol. 284 (2025) 137939.
[25] M. Murugesan, R. Mathiyalagan, Z.M. Ramadhania, J. Nahar, C.H. Luu, V.H. G. Phan, D.C. Yang, Q. Zhou, S. Chan Kang, T. Thambi, Tailoring hyaluronic acid hydrogels: impact of cross-linker length and density on skin rejuvenation as injectable dermal fillers and their potential effects on the MAPK signaling pathway suppression, Bioact. Mater. 49 (2025) 154–171.
[26] R. Mathiyalagan, M. Murugesan, Z.M. Ramadhania, J. Nahar, P. Manivasagan, V. Boopathi, E.-S. Jang, D.C. Yang, J. Conde, T. Thambi, Triterpenoid saponin-based supramolecular host-guest injectable hydrogels inhibit the growth of melanoma via ROS-mediated apoptosis, Mater. Sci. Eng.: R: Rep. 160 (2024) 100824.

[27] J. Delaey, P. Dubruel, S. Van Vlierberghe, Shape-memory polymers for biomedical applications, Adv. Funct. Mater. 30 (44) (2020) 1909047.
[28] X. Dou, G. Li, S. Wang, D. Shao, D. Wang, X. Deng, Y. Zhu, P. Gao, J. Liu, N. Deng, C. Yuan, Q. Zhou, Probiotic-loaded calcium alginate/fucoidan hydrogels for promoting oral ulcer healing, Int. J. Biol. Macromol. 244 (2023) 125273.
[29] L. Van Daele, S. Van Vlierberghe, P. Dubruel, Polymers for biomedical applications: the quest for treating cardiovascular diseases, Adv. Mater. 38 (7) (2026) e14833.
[30] L. Cao, W. Lu, A. Mata, K. Nishinari, Y. Fang, Egg-box model-based gelation of alginate and pectin: a review, Carbohydr. Polym. 242 (2020) 116389.
[31] F. Yu, P. Yang, Z. Yang, X. Zhang, J. Ma, Double-network hydrogel adsorbents for environmental applications, Chem. Eng. J. 426 (2021) 131900.
[32] V.H.G. Phan, B.-P.-T. Nguyen, N.Y. Nguyen, C.-N.-D. Tran, Q.-N.-D. Nguyen, C. H. Luu, P. Manivasagan, E.-S. Jang, D.C. Yang, D.U. Yang, Y. Li, J. Conde, T. Thambi, Longan-inspired chitosan-pectin core-shell hydrogel beads for oral delivery of biodrugs to enhance osteoporosis therapy, Int. J. Biol. Macromol. 308 (2025) 142254.
[33] G.M. Estrada-Villegas, G. Morselli, M.J.A. Oliveira, G. González-Pérez, A.B. Lugão, PVGA/Alginate-AgNPs hydrogel as absorbent biomaterial and its soil biodegradation behavior, Polym. Bull. 77 (8) (2020) 4147–4166.
[34] X. Jing, L. Chen, Y. Li, H. Yin, J. Chen, M. Su, F. Liu, T. Abdiryim, F. Xu, J. You, X. Liu, Synergistic effect between 0D CQDs and 2D MXene to enhance the photothermal conversion of hydrogel evaporators for efficient solar water evaporation, photothermal sensing and electricity generation, Small 20 (50) (2024) 2405587.
[35] A. Kumar, S.-Y. Won, A. Sood, S.-Y. Choi, R. Singhmar, R. Bhaskar, V. Kumar, S. M. Zo, S.-S. Han, Triple-networked hybrid hydrogels reinforced with montmorillonite clay and graphene nanoplatelets for soft and hard tissue regeneration, Int. J. Mol. Sci. 23 (22) (2022) 14158.
[36] V.H.G. Phan, H.-S. Duong, Q.-G.-T. Le, G. Janarthanan, S. Vijayavenkataraman, H.-N.-H. Nguyen, B.-P.-T. Nguyen, P. Manivasagan, E.-S. Jang, Y. Li, T. Thambi, Nanoengineered injectable hydrogels derived from layered double hydroxides and alginate for sustained release of protein therapeutics in tissue engineering applications, J. Nanobiotechnol. 21 (1) (2023) 405.
[37] A.A.d.N. Pomari, T.L.d.A. Montanheiro, C.P. de Siqueira, R.S. Silva, D.B. Tada, A. P. Lemes, Chitosan hydrogels crosslinked by Genipin and reinforced with cellulose nanocrystals: production and characterization, J. Compos. Sci. 3 (3) (2019) 84.
[38] N. Zhai, B. Wang, Preparation of fast-swelling porous superabsorbent hydrogels with high saline water absorbency under pressure by foaming and post surface crosslinking, Sci. Rep. 13 (1) (2023) 13815.
[39] R.R.A. Silva, C.S. Marques, T.R. Arruda, S.C. Teixeira, T.V. de Oliveira, Biodegradation of polymers: stages, measurement, standards and prospects, Macromol 3 (2) (2023) 371–399.
[40] F. Ng, V. Nicoulin, C. Peloso, S. Curia, J. Richard, A. Lopez-Noriega, *In vitro* and *in vivo* hydrolytic degradation behaviors of a drug-delivery system based on the blend of PEG and PLA copolymers, ACS Appl. Mater. Interfaces 15 (48) (2023) 55495–55509.
[41] J.L. Holloway, H. Ma, R. Rai, J.A. Burdick, Modulating hydrogel crosslink density and degradation to control bone morphogenetic protein delivery and in vivo bone formation, J. Control. Release 191 (2014) 63–70.
[42] K.Y. Lee, K.H. Bouhadir, D.J. Mooney, Controlled degradation of hydrogels using multi-functional cross-linking molecules, Biomaterials 25 (13) (2004) 2461–2466.
[43] S.A. Mathew, S. Arumainathan, Crosslinked Chitosan–Gelatin biocompatible nanocomposite as a neuro drug carrier, ACS Omega 7 (22) (2022) 18732–18744.
[44] C.J. Tormos, C. Abraham, S.V. Madihally, Improving the stability of chitosan–gelatin-based hydrogels for cell delivery using transglutaminase and controlled release of doxycycline, Drug Deliv. Transl. Res. 5 (6) (2015) 575–584.
[45] C. Lu, Z. Ling, C. Wang, J. Wang, Q. Yong, F. Chu, Multiple hydrogen bonding interactions toward rapidly self-healing, photothermal conversion elastomer composites, Compos. B Eng. 228 (2022) 109428.
[46] J.-H. Lee, T.-H. Lee, K.-S. Shim, J.-W. Park, H.-J. Kim, Y. Kim, S. Jung, Effect of crosslinking density on adhesion performance and flexibility properties of acrylic pressure sensitive adhesives for flexible display applications, Int. J. Adhes. Adhes. 74 (2017) 137–143.
[47] D. Zhang, L. Mei, Y. Hao, B. Yi, J. Hu, D. Wang, Y. Zhao, Z. Wang, H. Huang, Y. Xu, X. Deng, C. Li, X. Li, Q. Zhou, Y. Lu, A hydrogel-based first-aid tissue adhesive with effective hemostasis and anti-bacteria for trauma emergency management, Biomater. Res. 27 (1) (2023) 56.
[48] N. Duan, L. Mei, L. Hu, X. Yin, X. Wei, Y. Li, Q. Li, G. Zhao, Q. Zhou, Z. Du, Biomimetic, injectable, and self-healing hydrogels with sustained release of ranibizumab to treat retinal neovascularization, ACS Appl. Mater. Interfaces 15 (5) (2023) 6371–6384.
[49] Y. Li, X. Xuan, Z. Pan, Y. Li, T.Q. Do, V.H.G. Phan, H. Chen, T. Thambi, A robust and multifunctional conductive double-network hydrogel exhibiting self-healing, anti-freezing, antibacterial, and electromagnetic shielding properties for advanced wearable sensors and biofabrication, Chem. Eng. J. 522 (2025) 167264.
[50] H. Yin, L. Chen, F. Liu, T. Abdiryim, J. Chen, X. Jing, Y. Li, M. Su, X. Liu, MXene-based conductive hydrogels with toughness and self-healing enhancement by metal coordination for flexible electronic devices, Mater. Today Phys. 47 (2024) 101537.
[51] J. Zhao, X. Zhai, P. Li, X. Wang, Y. Wen, W. Xia, T. Luo, L. Wu, From sea cucumbers to soft robots: a photothermal-responsive hydrogel actuator with shape memory, ACS Appl. Mater. Interfaces 17 (4) (2025) 6979–6986.
[52] Y. Wang, Y. Miao, J. Zhang, J.P. Wu, T.B. Kirk, J. Xu, D. Ma, W. Xue, Three-dimensional printing of shape memory hydrogels with internal structure for drug delivery, Mater. Sci. Eng. C 84 (2018) 44–51.
[53] H. Xiao, C. Ma, X. Le, L. Wang, W. Lu, P. Theato, T. Hu, J. Zhang, T. Chen, A multiple shape memory hydrogel induced by reversible physical interactions at ambient condition, Polymers 138 (2017).
[54] M. Wang, B. Mo, B. Chen, L. Jiang, H. Yang, Self-healing quadruple-shape memory hydrogel based on imine, coordination, and borate bonds with tunable mechanical properties, Colloid Polym. Sci. 298 (3) (2020) 285–291.

SUPPLEMENTARY INFORMATION

Smart Multifunctional Hydrogels with Shape Memory, Conductivity, Self-Healing, and Adhesive Properties for Biomedical Applications

Ha Huong [a,b,1], Cuong Hung Luu [c,d,1], V. H. Giang Phan [a,1], Gopinathan Janarthanan [f], Ngoc-Thuy Huynh [a], Hieu Trung Nguyen [a], Nhu-Y Ngoc Ha [a], Hang Thu Ta [c,d], Qihui Zhou [e], Sanjairaj Vijayavenkataraman [f,g*], João Conde [h,*], and Thavasyappan Thambi [i,j,*]

[a] *Biomaterials and Nanotechnology Research Group, Faculty of Applied Sciences, Ton Duc Thang University, Ho Chi Minh City, Vietnam (phanvuhoanggiang@tdtu.edu.vn)*

[b] *Department of Advanced Materials Engineering, Kangwon National University, Samcheok 25931, Republic of Korea*

[c] *School of Environment and Science, Griffith University, Nathan, QLD 4111, Australia*

[d] *Queensland Quantum and Advanced Technologies Research Institute, Griffith University, Nathan, QLD 4111, Australia*

[e] *Shandong Engineering Research Center for Tissue Rehabilitation Materials and Devices, School of Rehabilitation Sciences and Engineering, University of Health and Rehabilitation Sciences, Qingdao, 266071, China*

[f] *The Vijay Lab, Division of Engineering, New York University Abu Dhabi, Abu Dhabi, United Arab Emirates*

[g] *Department of Mechanical and Aerospace Engineering, Tandon School of Engineering, New York University, Brooklyn, NY11201, USA*

[h] *Comprehensive Health Research Centre (CHRC), NOVA Medical School|Faculdade de Ciências Médicas, NMS|FCM, Universidade Nova de Lisboa, 1169-056 Lisboa, Portugal*

[i] *Graduate School of Biotechnology, College of Life Sciences, Kyung Hee University, Yongin si, Gyeonggi do 17104, Republic of Korea*

[j] *Department of Marine Biotechnology, AMET University, Chennai-603112, Tami Nadu, India*

[1] These authors contributed equally.

* Corresponding authors:

Thavasyappan Thambi, Ph.D., email: thambi@khu.ac.kr

João Conde, Ph.D., email: joao.conde@nms.unl.pt

Sanjairaj Vijayavenkataraman, Ph.D., email: vs89@nyu.edu

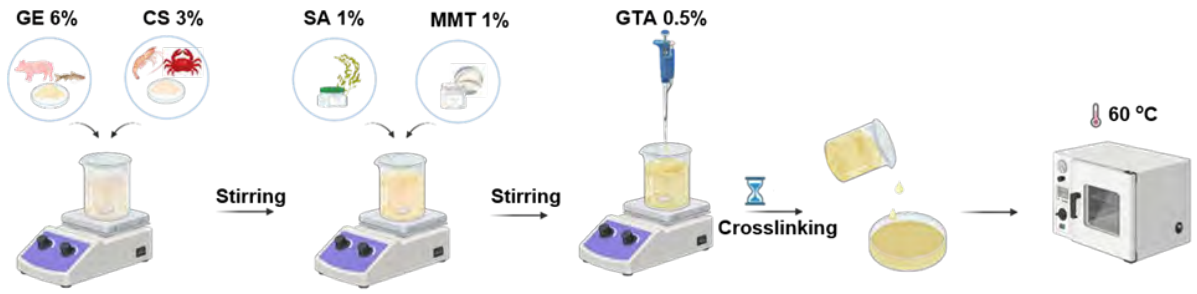

Scheme S1. Schematic representation of the SMH synthesis process.

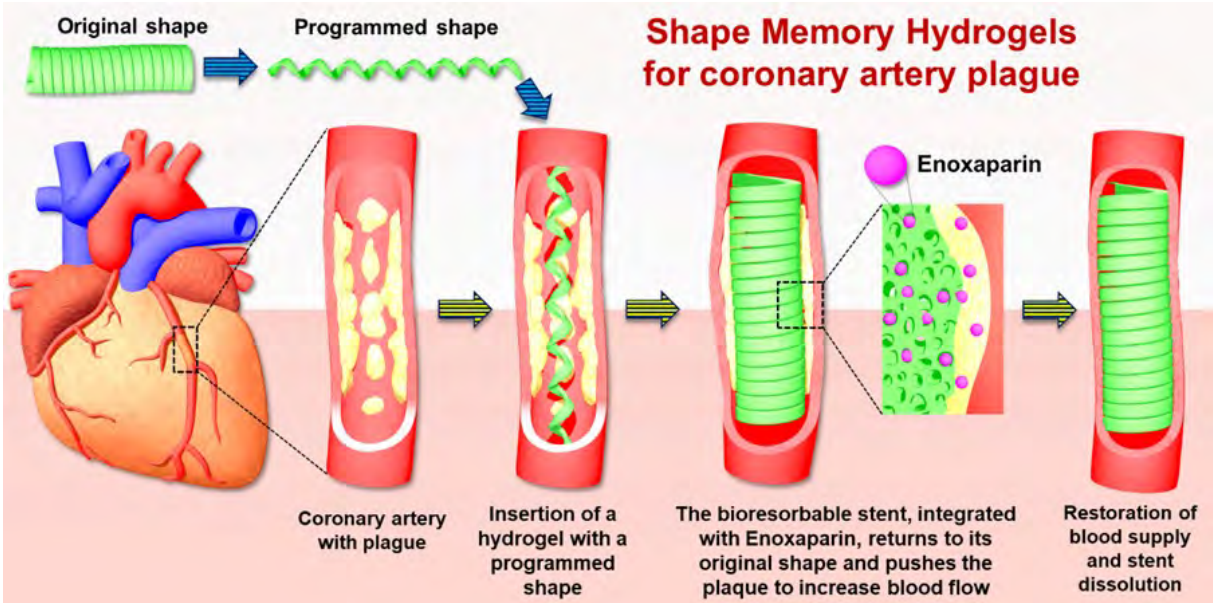

Scheme S2. Illustration of the potential application of shape memory hydrogel stents for the treatment of coronary artery plaque. The hydrogel stent is initially programmed into a compact shape for minimally invasive insertion into the narrowed artery. Upon deployment, the stent recovers its original expanded shape, exerting mechanical force to compress the plaque and restore blood flow. The bioresorbable stent is integrated with enoxaparin, which is locally released to prevent blood clot formation. Over time, the hydrogel stent gradually dissolves, eliminating the need for surgical removal and promoting vessel healing.

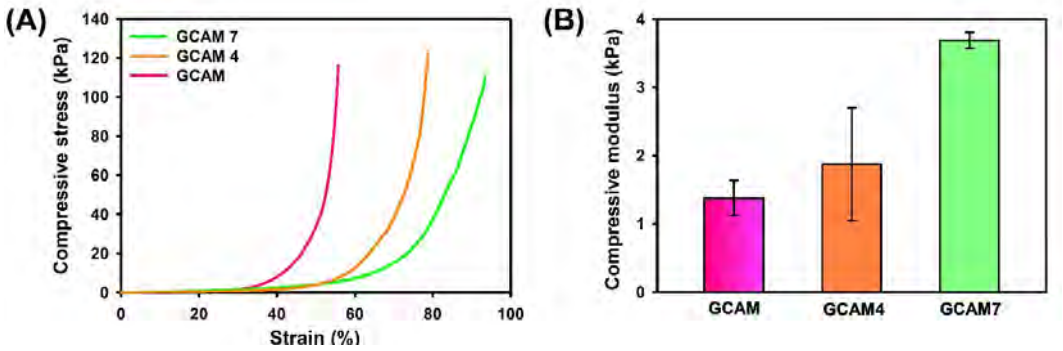

Figure S1. Mechanical properties of hydrogels. **(A)** Compression stress–strain curves of GCAMs, and **(B)** their corresponding compressive modulus values.

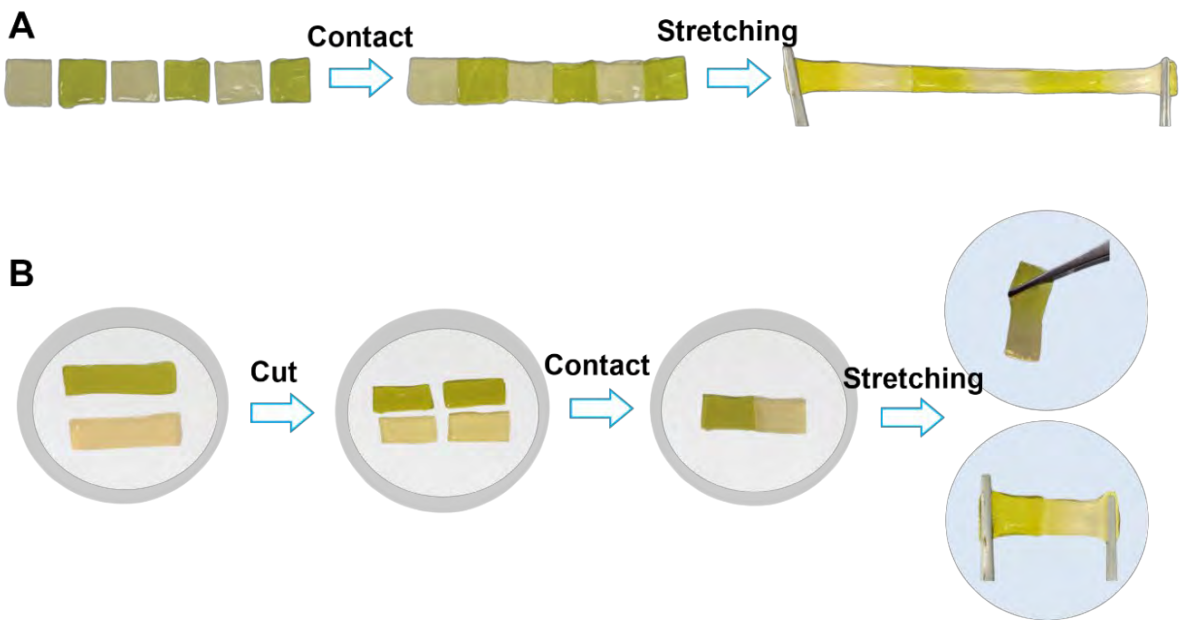

Figure S2. Photographic demonstration of the self-healing behavior of GCAM7 hydrogel. **(A)** Sequential healing of multiple cut hydrogel pieces into a single, integrated strip capable of being suspended between two supports. **(B)** Healing of two differently colored hydrogel segments after cutting and recontacting, followed by lifting and hanging tests, illustrating restoration of integrity and mechanical strength.

Figure S3. Electrical self-healing behavior of the GCAM7 hydrogel conductor. The sequence shows cutting, self-healing, and subsequent stretching of a damaged hydrogel strip while the LED remains lit, demonstrating restoration of conductivity after healing.

Figure S4. Optical images and SEM micrograph of cut and self-healed specimens, in which the fracture interface disappears, and the porous network becomes continuous, providing visual evidence of the reconstructed microstructure.

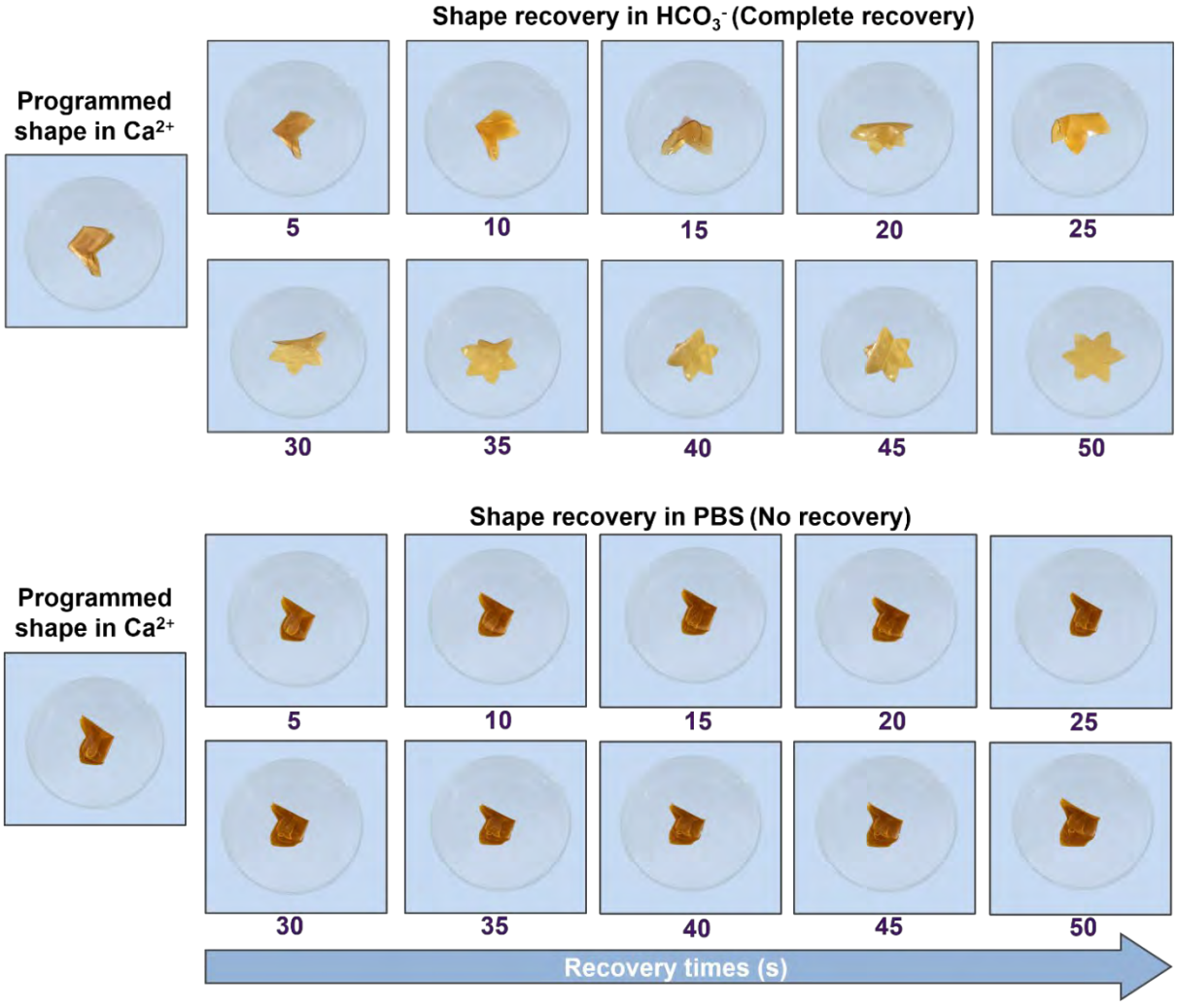

Figure S5. Time-dependent shape recovery of flower shaped GCAM7 hydrogels programmed in calcium ion and immersed either in bicarbonate solution or PBS.

Table S1. Release kinetics of GCAM hydrogels.

	GCAM		GCAM4		GCAM7	
Fitting models	**Regression equations**	**R^2**	**Regression equations**	**R^2**	**Regression equations**	**R^2**
Zero-order	$Q = 0.0028\ t + 0.1684$	0.9847	$Q = 0.0023\ t + 0.1237$	0.9950	$Q = 0.0027\ t + 0.1507$	0.9921
First-order	$\log Q = 0.0021\ t - 0.5823$	0.9917	$\log Q = 0.0023\ t - 0.7110$	0.9757	$\log Q = 0.0022\ t - 0.6306$	0.9751
Higuchi	$Q = 6.2127\ t^{1/2} - 13.2715$	0.9308	$Q = 5.0295\ t^{1/2} - 12.3535$	0.9591	$Q = 5.9397\ t^{1/2} - 14.1112$	0.9554
Hixson–Crowell	$Q^{1/3} = -0.0126\ t + 5.0285$	0.7775	$Q^{1/3} = -0.0057\ t + 4.5723$	0.9721	$Q^{1/3} = -0.0082\ t + 4.6589$	0.9530
Korsmeyer–Peppas	$\log Q = 0.3659 \log t - 1.0821$	0.9008	$\log Q = 0.5066 \log t - 1.4528$	0.9744	$\log Q = 0.4660 \log t - 1.3028$	0.9446

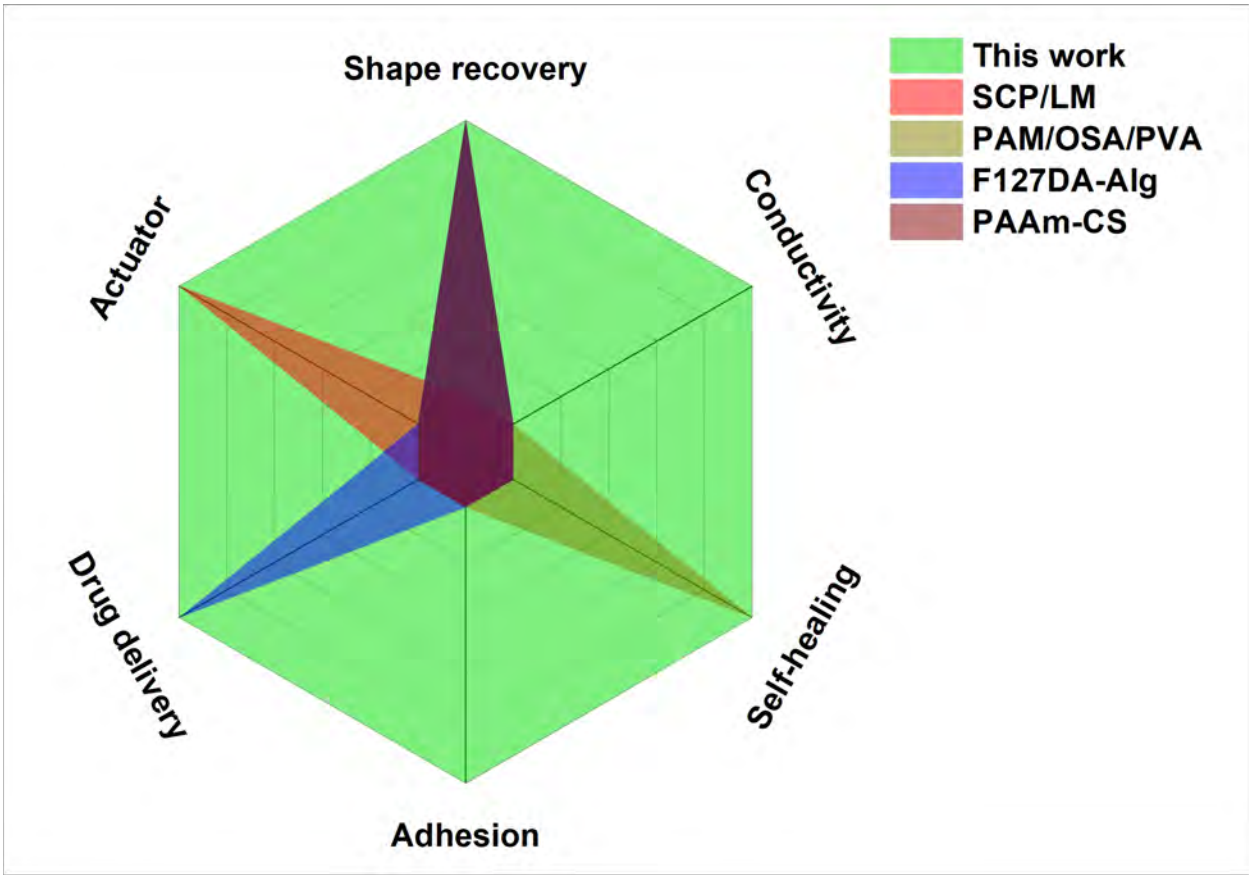

Figure S6. Radar plot comparing the overall performance of GCAM7 with representative recently reported hydrogels. The six normalized axes correspond to shape fixity ratio, final shape recovery ratio, recovery time, tensile strength, self-healing efficiency, and adhesive strength or electrical conductivity. GCAM7 encloses the largest area on the plot, indicating its more balanced combination of rapid and nearly complete shape recovery, mechanical robustness, and additional functional properties relative to the comparison hydrogels.